Visualising UV-A light-induced damage to plasma membranes of eye lens

Peter S. Sherin,[1,2*] Aurimas Vyšniauskas,[3,4] Ismael López-Duarte,[1] Peter R. Ogilby,[5] Marina K. Kuimova[1*]

[1] Chemistry Department, Molecular Sciences Research Hub, Imperial College London, 82 Wood Lane, London, W12 0BZ, UK
[2] International Tomography Center SB RAS, Institutskaya street 3A, Novosibirsk, 630090, Russia
[3] Center for Physical Sciences and Technology, Saulėtekio av. 3, Vilnius, LT-10257, Lithuania
[4] Chemistry Department, Vilnius University, Naugarduko st. 24, Vilnius, LT-03225, Lithuania
[5] Department of Chemistry, Aarhus University, Langelandsgade 140, Aarhus, DK-8000, Denmark

Abstract

An eye lens is constantly exposed to the solar UV radiation, which is considered the most important external source of age-related changes to eye lens constituents. The accumulation of modifications of proteins and lipids with age can eventually lead to the development of progressive lens opacifications, such as cataracts. Though the impact of solar UV radiation on the structure and function of proteins is actively studied, little is known about the effect of photodamage on plasma membranes of lens cells. In this work we exploit Fluorescence Lifetime Imaging Microscopy (FLIM), together with microviscosity-sensitive fluorophores termed molecular rotors, to study the changes in viscosity of plasma membranes of porcine eye lens resulting from two different types of photodamage: Type I (electron transfer) and Type II (singlet oxygen) reactions. We demonstrate that these two types of photodamage result in clearly distinct changes in viscosity – a decrease in the case of Type I damage and an increase in the case of Type II processes. Finally, to simulate age-related changes that occur *in vivo*, we expose an intact eye lens to UV-A light under anaerobic conditions. The observed decrease in viscosity within plasma membranes is consistent with the ability of eye lens constituents to sensitize Type I photodamage under natural irradiation conditions. These changes are likely to alter the transport of metabolites and predispose the whole tissue to the development of pathological processes such as cataracts.

Keywords: Eye lens, plasma membranes, viscosity, molecular rotors, UV-A light, kynurenic acid.

*Corresponding authors:
Dr Petr S. Sherin, p.sherin@imperial.ac.uk
Dr Marina K. Kuimova, m.kuimova@imperial.ac.uk

Introduction

The eye lens has a unique structure, mainly consisting of organelle-free long fibre cells packed in an onion-like construction [1]. This structure is necessary to support the main functions of an eye lens, the transmittance and focusing of visible light onto the retina. To minimize scattering and increase the acuity of vision, the lens cells are tightly packed, with small intercellular space and thin plasma membranes, which are smaller than the wavelength of transmitted light. In avascular tissue of eye lens the transport of metabolites proceeds *via* plasma membranes, hence, any defects in their structures could induce the development of disorders, including some types of cataracts [1].

The absence of organelles in eye lens cells has important consequences, leading to no protein [2] and lipid [3] turnover during a lifespan of an individual. All eye lens constituents accumulate various modifications with age, and this manifests itself in an increased light scattering, yellow coloration and lens stiffness. A formation of a barrier preventing metabolite exchange between central and peripheral areas of lens was reported [4,5], which predisposes the lens nucleus to oxidative stress and, hence, cataract formation [6]. Though significant age-related changes in lipid content of human lens cell membranes were reported [7,8], a mechanism for the diffusion barrier formation is still unclear. An investigation of age- and oxidation damage-related changes in plasma membranes could shed light on the mechanisms of eye lens aging and the formation of cataracts.

The most important external source of damage to proteins and lipids of eye lens is UV-A radiation (315-400 nm) [9,10], the most intense part of the solar UV radiation reaching the Earth's surface. In a human lens this light could be absorbed by endogenous chromophores, mainly kynurenine (KN) and its derivatives [11,12]. Though KNs exhibit low yields of reactive triplet states [13,14], they could nevertheless still induce damage to proteins *via* direct one-electron oxidation (Type I) [15,16] or *via* the formation of singlet oxygen (Type II) [17,18] and its subsequent reactions with surrounding molecules. It should be noted that an eye lens is the tissue with extremely low presence of oxygen, at the level below 2 μM (or PO_2 < 2 mmHg) in the lens nucleus [19] (*cf* PO_2 38 mmHg, *ca*. 5% of atmospheric pressure in the aqueous humor around lens [19], and near atmospheric pressure in epithelial skin cells). In a tissue with such a low oxygen content, Type I reactions may be expected to dominate. Proteins are currently considered to be the major targets for photodamage due to their abundance, however, a possibility of Type I processes (intracellular or intramembrane), leading to plasma membrane damage, has not yet been explored.

In our previous work we have shown that Fluorescence Lifetime Imaging Microscopy (FLIM) together with small fluorescent molecules sensitive to local microviscosity, the so-called 'molecular rotors', is a powerful non-destructive approach to study the properties of plasma membranes of eye lens cells [20]. The advantage of a lifetime-based approach is its independence of the sensor concentration, unlike in fluorescence intensity-based methods. In our pilot study of porcine eye lens membranes, we discovered that they exhibited extremely high viscosities and high degree of lipid self-organization, as compared to several other cell types studied to date [21-24]. These high viscosities, consistent with lipids present in pure liquid ordered (L_o) phase, originate from the high cholesterol and sphingomyelin content within plasma membranes of eye lens [25, 26]. It seems likely that any damage to these well-organized membranes may significantly alter their structure and, therefore, may affect their functionality.

Here we use FLIM in combination with a charged BODIPY-based molecular rotor to investigate the consequences and dynamics of different types of photodamage (Type I and Type II) on the plasma membrane viscosity in porcine eye lens cells. We induce photodamage in a microscopy experiment in a spatially resolved manner [27-29] and visualise affected tissues in direct comparison

with neighbouring non-affected areas. To simulate all possible types of photodamage originating from intrinsic porcine eye lens chromophores under natural ageing conditions we photolyse the whole eye lens under anaerobic conditions using 355 nm irradiation. Subsequent analysis of viscosities in lens slices indicate a viscosity decrease under these conditions, consistent with Type I reactions. Our data demonstrate the versatility of FLIM-molecular rotor approach to study the impact of different sources of photodamage to these unique tissues on the cellular level.

Experimental section

Materials

The synthesis of BODIPY rotors **B3++** [24], **B6++** [30], **B10++** [31] and **B10** [21] was reported previously. Kynurenic acid from Sigma-Aldrich (purity > 98%) was used as received. All solvents used were spectroscopic grade. Toluene, methanol and DMSO were obtained from Sigma-Aldrich, glycerol was obtained from Alfa-Aesar, alpha-tocopherol from FluoroChem-UK, deuterated water from Goss Scientific Ltd.

Preparation of eye lens slices

Enucleated porcine eyes were obtained from the abattoir near Bedford, UK, within one hour after animal's death and stored on ice for less than 2 hours. The extracted lenses were weighed and measured, and either immediately frozen or subjected to the 355 nm photolysis as a whole lens (*vide infra*) and consequently frozen. All lenses were stored at -80 °C until used in experiments, typically 2-6 days after extraction. Slices of lenses with thickness of 14 μm from equatorial area were obtained by cryotome slicing (OTF cryostat, Bright Instrument Company Ltd, UK) and mounted onto microscope slides (SuperFrost Plus, Thermo Fisher Scientific, Germany). The total number of used animal lenses was N = 24; the age of animals was around 6 months.

UV-A photolysis of the whole eye lenses

Whole eye lenses were placed in 1x1 cm quartz cells with 2 ml of artificial aqueous humor (AAH), a solution similar to the aqueous humor in the anterior chamber of the eye. The AAH was made from NaCl 130 mM; KCl 5 mM; $MgCl_2$ 0.5 mM; $CaCl_2$ 1 mM; $NaHCO_3$ 10 mM; glucose 5 mM; buffered with 10 mM HEPES. The anaerobic conditions were achieved by intensive bubbling of nitrogen through the solution 30 min prior to and during the photolysis. For aerobic conditions, the lens was placed in cell for 30 min with air equilibrated AAH. The whole lenses were photolyzed for 30 min at 355 nm (Nd:YAG, Surelite 1, Photonic Solutions, pulse duration 5 ns, pulse energy 3 mJ, 10 Hz, beam diameter 8 mm). Control lenses were kept in deaerated AAH for one hour, without UV-A radiation. Three lenses were used for each type of experiments, including controls.

Incubation of eye lens slices with fluorescent dyes

Phosphate buffered saline (PBS) from Invitrogen was used in all experiments. Each fluorescent dye was dissolved in DMSO at the concentration of 3 mM and stored at -20 °C. PBS solutions of a dye at 10 μM were prepared immediately before staining of eye lens slices by adding of 0.2 μl of DMSO stock solution in 60 μl of PBS; the resulting total concentration of DMSO was 0.3% by volume. Each eye lens slice was stained with 8 μl of a 10 μM PBS dye solution for 10 minutes. After the removal of the excess of PBS with a gentle application of a filter paper, the lens slices were covered by a cover slip and sealed with non-fluorescent lacquer to avoid the drying of tissue slices during the data acquisition. In our experiments we used lenses from young animals that have no

differences in lipid composition between the cortex and the nuclear regions of the lens [32]. Thus, frames for the acquisition of fluorescent time-resolved signal were chosen randomly in a slice.

Measurement of singlet oxygen quantum yields

The BODIPY fluorophores' ability to photosensitize singlet oxygen was quantified in air-saturated toluene, methanol and a 70% glycerol / 30% methanol mixture (v/v%). Additional measurements were performed in oxygen-saturated toluene and methanol. Quantum yields of singlet oxygen production, φ_{Δ}, in toluene and methanol were obtained by comparing the magnitude of the BODIPY-sensitized time-resolved singlet oxygen phosphorescence signal to the signal sensitized by phenalenone, which was used as the standard and dissolved in the same solvent as the BODIPY fluorophore. The singlet oxygen quantum yields of phenalenone are $\varphi_{\Delta} = 0.92 \pm 0.03$ in both methanol and toluene [33]. Phenalenone in methanol was used as a standard for experiments in methanol-glycerol mixtures with the correction of signal intensities for differences in the efficiency of light collection due to a change in the solvent refractive index (a factor of n^2). Moreover, using the empirical correlation between the solvent refractive index and the solvent-dependent rate constant for singlet oxygen radiative decay, the signal intensities were likewise corrected [34]. For all measurements, the oxygen phosphorescence signal was recorded using different excitation powers, and the integrated signal intensities were plotted against the excitation power. The quantum yield was calculated using the following equation [34]:

$$\varphi_{\Delta,\mathrm{s}} = \varphi_{\Delta,\mathrm{st}} \frac{\tau_{st} k_s (1-10^{-A_{st}})}{\tau_s k_{st} (1-10^{-A_s})} \qquad (1)$$

where $\varphi_{\Delta,s}$ and $\varphi_{\Delta,st}$ are singlet oxygen quantum yields of the sample and the standard, respectively, τ_{st} and τ_s are the lifetimes of singlet oxygen, k_{st} and k_s are the slopes of the intensity vs. power plots, and A_{st} and A_s are the absorbances obtained by integrating the product of the absorption spectrum and the normalized laser spectrum. The absorbances of sample and standard were measured using a Shimazu UV3600 spectrometer and were set to approximately 0.1. The excitation was performed using a Tsunami 3941 Ti:Sapphire femtosecond laser (Spectra Physics), which was pumped by a Millenia V Nd:VO_4 laser (Spectra Physics). The output pulses were amplified by a Spitfire regenerative amplifier (Spectra Physics), which increases the pulse energy by a factor of 10 and reduces the pulsing frequency to 1 kHz. The regenerative amplifier was pumped by an Evolution Nd:YLF laser (Spectra Physics). The output of the Spitfire amplifier was frequency doubled using a β-barium borate (BBO) crystal. The resulting 380 nm wavelength was used for exciting the samples and the standard. As previously described [35] the time-resolved singlet oxygen phosphorescence at 1275 nm was recorded using a cooled PMT sensitive in the near-IR that was operated in a photon counting mode. In all experiments a 1 cm quartz cuvettes were used.

Fluorescence imaging

Multiphoton fluorescence imaging of eye lens slices stained with various dyes was performed using a confocal laser-scanning microscope Leica TCS SP5 II (Leica Microsystem Ltd, Germany). Room temperature imaging was carried out with a x100 (N.A. 1.0) HCX PL APO CS oil immersion objective lens with a correction collar (11506279, Leica Microsystem Ltd, Germany). Samples were excited at 930 nm with a Ti:Sapphire pulsed laser source (680-1080 nm, 80 MHz, 140 fs, Chameleon Vision II, Coherent Inc., Germany) and the emission intensity was recorded at 490-700 nm for all dyes.

Fluorescence lifetime imaging (FLIM)

FLIM images of 512×512 pixels were obtained using a Leica TCS SP5 II inverted scanning confocal microscope coupled with a TCSPC module SPC830 (Becker&Hickl, Germany) and internal FLIM detector PMH-100 (Becker&Hickl, Germany), synchronised to a Ti:Sapphire pulsed laser source (680-1080 nm, 80 MHz, 140 fs, Chameleon Vision II, Coherent Inc., Germany).

Excitation was performed at 930 nm for all BODIPY-based rotors and the emission was captured at two wavelength ranges to check for possible dye aggregation: 500-580 nm (monomers) and 590-670 nm (aggregates). The laser power was maintained at < 80 mV before entering the microscope to avoid cell damage. The acquisition time was varied in the range 200-500 s depending on the emission intensity from each dye.

FLIM data was analysed in SPCImage v.8.3 software (Becker&Hickl, Germany) using a model of incomplete biexponential decay with offset values fixed to zero. Maximum Likelihood Entropy (MLE) was used as a fitting algorithm, particularly suitable for low-intensity signals [36]. The binning of pixels (rectangular bin 3, 7x7 pixels) was used for all data to produce a typical peak count in the decay maximum in the range 100-200 counts per pixel (which is deemed sufficient for the MLE analysis); thresholding was adjusted from sample to sample to remove pixels of low intensity from the analysis. A pseudocolour scale was assigned to each fluorescence lifetime, amplitude and the goodness of fit (χ^2) values (red for small values and blue for large values) to provide corresponding lifetime maps. The lifetimes and deviations presented in the text are the mean values and standard deviations calculated from averaged histograms (4-6 for each experiment and plotted based on the total amount of pixels around 300 000).

Results and discussion

Choice of molecular rotor

BODIPY-based molecular rotors are hydrophobic molecules, which easily stain plasma membranes in 2D cell culture [21, 37], however, their use in 3D culture, such as spheroids or tissue slices is more challenging due to poor aqueous solubility and resulting accessibility issues [20, 38, 39]. To address the issue of poor aqueous solubility, a series of dyes with charged groups and decreasing length of the aliphatic tail were synthesised in our group [20, 24, 30, 31] (see Chart S1 of Supporting Information, SI, for chemical structures). Previously, we found that only one of these molecules, **BC3+**, efficiently penetrated the unusually rigid membranes of eye lens cells without aggregation [20], however, this dye produced insufficiently bright images that required long accumulation times. We now optimised the staining protocol to minimize the time between the medium preparation and tissue immersion, from tens of minutes to tens of seconds. Under these optimized conditions we confirmed that all available rotors do not show aggregation (Section S1 of SI). The rotor **B6++** (see Chart 1 for chemical structure), gave the brightest signal at these conditions (Figure S2 of SI) and was chosen as the main dye for the present work.

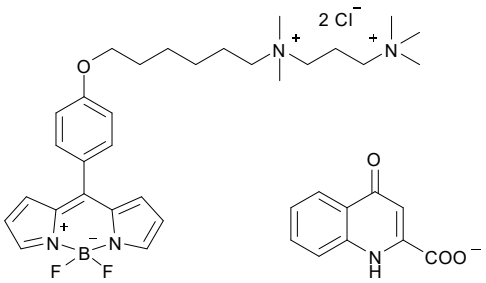

B6++ **KNA**

Chart 1. Molecular structures of fluorescent molecular rotor **B6++** and an intrinsic photosensitiser found in human eye in trace amounts, KNA.

Our FLIM data have shown that following excitation all BODIPY-based molecular rotors exhibit a two-component excited state decay within eye lens membranes. Similarly to our previous studies, [20, 40] biexponential decay could be assigned to two different orientations of rotors, typical for systems with high degree of lipid ordering, such as liquid-ordered (L_o) or gel-phases [40]. The shorter component (τ_1 = 0.97 ± 0.09 ns) could be assigned to molecules localised in the lipid headgroup region of membrane and the longest component (τ_2 = 4.22 ± 0.20 ns) to those within the tail region of lipid bilayer (lifetimes in parenthesis are data for **B6++**). The longer-lived component should accurately represent the viscosity and the diffusivity within such membranes [20, 40]. The direct comparison of viscosities obtained in this study to our previous work using **B3+** in given in Section S2 of SI.

Type-II photodamage

To record FLIM images of viscosity distribution in membranes of eye lenses, we used multiphoton excitation at 930 nm from Ti:Sapphire laser of **B6++**. Unexpectedly, we found that relatively high powers and long acquisition times needed to achieve high signal/noise images lead to a significant increase of fluorescence intensity and lifetime from the membranes within the irradiated area, Figure 1. A typical time-resolved decay trace recorded from a plasma membrane location before and after irradiation are shown as grey and blue curves, respectively, Figure 1E. The analysis of the FLIM data shows that 930 nm irradiation leads to an increase in both the amplitude (A_2) and the lifetime (τ_2) of the long decay component, consistent with the increased viscosity of the irradiated area (Figures 1F-1H).

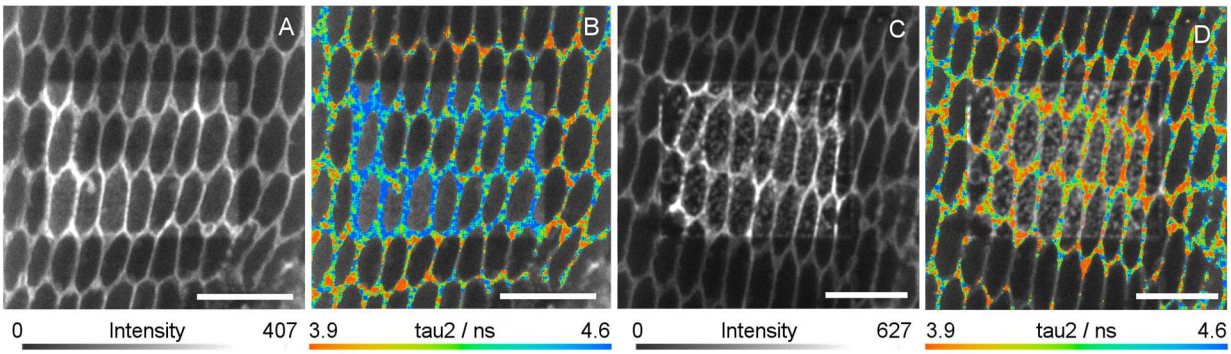

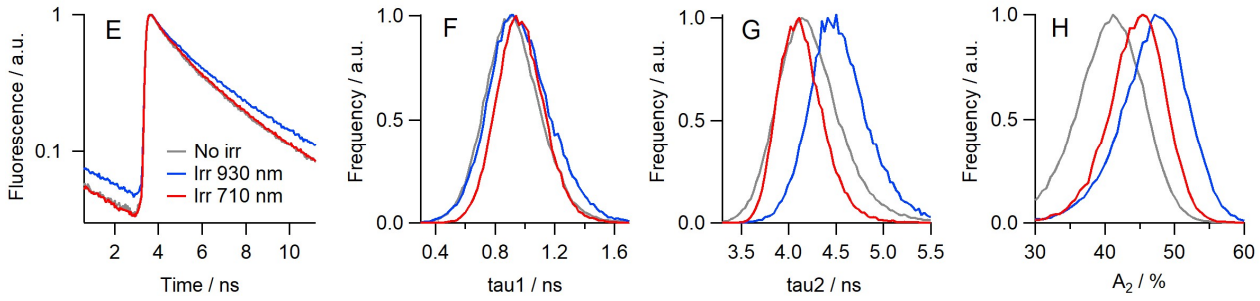

Figure 1. (A, C) Intensity and (B, D) FLIM images of porcine eye lens stained with 10 μM **B6++** following (A, B) 930 nm irradiation or (C, D) in the presence of 3 mM KNA following 710 nm irradiation. The central frame was irradiated for 1400 sec at 2.0 mW power at the wavelength indicated, the whole image acquisition time was 300 sec at 0.45 mW. Scale bars are 10 μm. (E-H) FLIM analysis of the data. (E) Averaged time-resolved decays recorded for **B6++** from randomly selected plasma membrane locations (see Section S1 of SI for additional details). Distributions of τ_1 (F), τ_2 (G) and A_2 (H) obtained from biexponential fits of FLIM data. No irradiation (grey lines), 930 nm irradiation (red lines) and 710 nm irradiation in the presence of KNA (blue lines). Independent biological experiments were performed in triplicate, two image frames were analysed per experiment. Full size images are presented in Figure S6 of SI.

While this increase of viscosity was unexpected, we note that a large viscosity increase in model and plasma membranes was previously reported because of singlet oxygen mediated Type II photoreactions [27-29]. To collect evidence for Type II photoreactions taking place in our present samples, we carried out three control experiments.

In the first experiment, the eye lens slices were stained with **B6++** in heavy water (D_2O). In D_2O, the solvent-mediated lifetime of singlet oxygen increases from 3.5 to 69 μs [41, 42]. In turn, the yield of kinetically competing Type II photodamage should increase in D_2O. Conversely, H/D isotope effects typically have no influence on electron transfer reactions and a significant slowdown is expected in the case of hydrogen atom transfer (both these processes are Type I photooxidation reactions) [43]. We expect a significant exchange of H_2O to D_2O within the tissue in these experiments. Accordingly, a larger increase in fluorescence intensity (Figure S7 of SI) and fluorescence lifetime (τ_2, Figure 2C) were observed upon irradiation of eye lens slices incubated in D_2O compared to H_2O. This lends evidence that the changes in **B6++** fluorescence were, indeed, due to singlet oxygen reactions.

In the second experiment, we added 10 μM of α-tocopherol as an efficient quencher of singlet oxygen with the rate constants of between 5×10^7 to 7×10^8 $M^{-1}s^{-1}$ depending on solvent [41] in the staining solution together with **B6++**. We noted a slight distortion of eye lens membranes upon α-tocopherol inclusion (Figure S8 of SI) followed by an increase of their viscosity (light blue curve, Figure 2D). However, the photolysis at 930 nm resulted in only a minor change of lens viscosity. It is known that α-tocopherol can also trap radicals, albeit with lower rates, *e.g.* 6×10^3 M^{-1} s^{-1} with hydroperoxide in phospholipid bilayers [44]. Our results imply the efficient quenching of reactive species by α-tocopherol, again, lending support for Type II reactions taking place.

In the third experiment, FLIM images were recorded with eye lens slices stained with **B6++** and sodium azide (NaN_3), an efficient quencher of both singlet oxygen and triplet excited states that are generally the precursors in the photosensitized production of singlet oxygen [41]. Our experiments were performed at a NaN_3 concentration high enough to mitigate singlet oxygen reactivity in the

cellular environment (10-40 mM) [28]. After exposure of samples with/without NaN_3 to the same dose of irradiation at 930 nm, we confirmed that 10 mM NaN_3 significantly reduces the photodamage and presence of 40 mM NaN_3 almost completely inhibits it, as shown by mild or insignificant increase of τ_2 value after photolysis, Figure 2E.

Taken together, these three experiments imply that the mechanism of observed photodamage contains an appreciable component of Type II chemistry involving singlet oxygen.

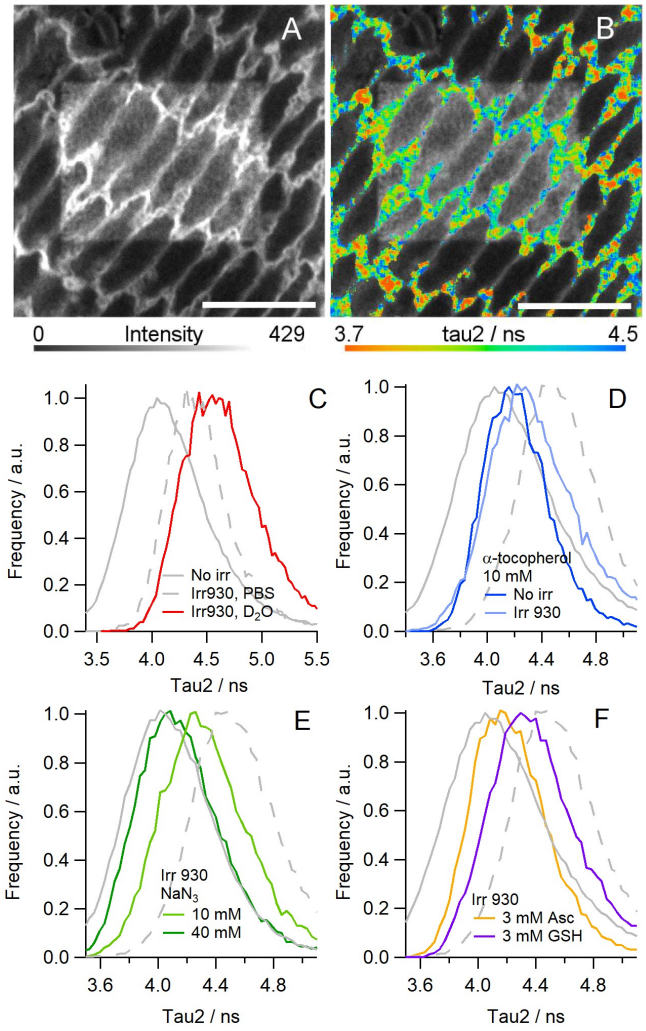

Figure 2. Intensity (A) and FLIM (B) images of porcine eye lens stained with 10 μM **B6++** and 3 mM Asc following 930 nm irradiation. The central frame was irradiated for 1400 sec (at 2.0 mW power), the whole image acquisition time was 300 sec (at 0.45 mW). Scale bars are 10 μm. (C-F) Distributions of τ_2 obtained from biexponential fits of FLIM data. Before (solid grey) and after (dashed grey lines) photolysis at 930 nm in the absence and presence of (C) D_2O (red lines), (D) 10 μM of α-tocopherol (blue lines), (E) 10 mM (green lines) and 40 mM (olive lines) NaN_3, (F) 3 mM Asc (orange) and 3 mM GSH (violet). Independent biological experiments were performed in duplicate, two image frames were analysed per experiment.

Origin and prevention of Type II photodamage

Viscosity increases during Type II photooxidation reactions were previously studied in giant unilamelar vesicles, GUVs, constructed from the unsaturated lipid, 1,2-dioleoyl-sn-glycero-3-phophocholine (DOPC), containing porphyrin-based photosensitiser [29]. This increase was in

agreement with earlier reports of an increase in intracellular viscosity upon singlet-oxygen induced oxidation in live cells, also containing porphyrin-based photosensitisers [27, 28]. In the case of eye lens cells, our data above indicate that, upon 930 nm irradiation, a similar viscosity increase is taking place, however, the source of singlet oxygen is less clear.

The porcine eye lens has a significant absorption in the UV-A region (Figure S5 of SI) but this absorption is not assigned to any particular endogenous chromophore(s). Extrapolation of data reported for human and other animal lenses [11, 12, 45, 46] allows to assume the contributions from KNs and NAD(P)H as the main UV-A absorbing metabolites. These molecules are mostly photochemically inert, but, under UV-A irradiation, KNs are able to generate triplet states [12, 13], while NAD(P)H can photoionize [47] with low yields. Though proteins could also contribute to this absorption [48], their photochemistry under UV-A light is currently unknown.

BODIPY-based dyes were reported to have negligible singlet oxygen quantum yields, unless modified with heavy atom substituents, such as iodine or, to a lesser extent, bromine [49, 50]. Our own experiments (Section S3 of SI), indicate that **B10**, one of close analogues of **B6++**, has quantum yields of singlet oxygen production of less than 1% in all organic solvents studied, both viscous and non-viscous, Table S1 of SI. At the same time, there are reports of cell damage and death upon multiphoton irradiation of cell cultures at 800-900 nm [51, 52]. Therefore, the photodamage seen upon 930 nm irradiation could be due to multiphoton induced reactions of the BODIPY excited state rotor or from endogenous chromophores. It should also be noted that the photodegradation products of endogenous chromophores may be more efficient generators of singlet oxygen. Due to the nature of our setup (coverslip-sealed tissue sections), **B6++** has to be added to the sample prior to irradiation and so it is impossible to test whether the photodamage still occurs in the absence of the dye. Irrespective of the source of the singlet oxygen, our experiments indicate that, similar to model unsaturated membranes [29] and to cultured mammalian cells [27, 28], Type II reactions appear to result in an increase of a lipid membrane viscosity, even in an extremely rigid environment of eye lens plasma membranes.

It should be noted that τ_2 value increases gradually over exposure and within the irradiated frame only, leaving the area outside irradiation frame unaffected. It is known that singlet oxygen reacts with unsaturated lipids *via* double bonds forming hydrophilic hydroxyperoxide units [53, 54]. No evidence for significant diffusion of singlet oxygen (or its products) outside an irradiated frame seen here is consistent with previous observations with limited propagation of singlet oxygen damage in the case of GUVs suspended in aqueous solution [29] and lipid droplets in oil-in-water emulsions [55]. However, in the case of GUVs, irradiation of a small part of a vesicle caused the whole vesicle to equilibrate to a higher viscosity value. We do not see such diffusion of oxidised species across eye lens cells, presumably due to a higher viscosity of these membranes (1000 cP [20]) compared to that of DOPC GUVs, *ca.* 170 cP [29].

The eye lenses of mammals contain high concentrations of natural antioxidants, such as ascorbate (Asc) and glutathione (GSH), at levels of few mM [11, 56]. To test whether these antioxidants are able to inhibit Type II photodamage, the eye lens slices were stained with additional Asc or GSH, at 3 mM, close to physiological concentrations. Indeed, the presence of antioxidants reduced an increase of τ_2 during photolysis (Figure 2B) and this protective effect was more pronounced in the case of Asc. Both Asc and GSH are reported to be relatively weak quenchers of singlet oxygen (approx. 2×10^6 $M^{-1}s^{-1}$ in D_2O [41, 57]). Asc is also known as an effective quencher of triplet states of KN and its derivatives, with rate constants (1-2) $\times$ 10^9 $M^{-1}s^{-1}$ [15, 58, 59], and GSH is known as a scavenger of free radicals [60, 61]. However, the rate constants of different reactions

could be significantly affected by the complex environment of eye lens tissue. The combination of quenching reactions may contribute to the observed prevention of Type II damage.

As reported in [19], the eye lens is almost oxygen-free tissue. However, the intralenticular levels of O_2 may increase in epithelial and cortical cells, the most exposed to the outer layer of a lens, due to an age-related damage to mitochondria, as reported for mice and rat lenses [62,63]. Though human lenses are significantly different from rodent lenses by composition [25, 26] and structure [1], some contribution from Type II reactions to the total damage to plasma membranes in aged and cataractous human lenses could not be excluded.

Type I photodamage

Next, we stained the porcine eye lens with an effective photosensitizer, kynurenic acid (KNA, see Chart 1 for chemical structure), which is present in trace amounts in healthy human (but not porcine) eye lenses and at elevated quantities in cataractous lenses [64]. As an intrinsic eye lens component, we expected good permeability of this molecule across plasma membranes with homogeneous distribution within intracellular space. Unfortunately, the location of this molecule within eye lens slice could not be detected, due to an extremely low quantum yield of fluorescence, *ca.* 1% [65].

We expect two photon excitation at 710 nm to produce triplet states of KNA, which has a sufficient linear absorption at 355 nm [65]. An example of FLIM image obtained after 710 nm irradiation of the eye lens slice stained with 3 mM KNA and 10 μM **B6++** is given in Figure 1C (see Figure S6 of SI for the full-size image). No visual changes in the structure of plasma membranes were detected, while drastic change of the intracellular space morphology was seen, showing the formation of granular inclusions stained with **B6++**.

The analysis of FLIM data in cellular membranes revealed a shift of τ_2 distribution to shorter values (Figure 1G) with an increase of its amplitude (A_2, Figure 1H). The lower values of τ_2 seen upon 710 nm photolysis are in contrast with the larger τ_2 values seen upon 930 nm irradiation, which we assigned to Type II photodamage. Despite the shortening of τ_2, we observed an increase of fluorescence intensity from irradiated area (Figure 1C), which is primarily due to the increase of A_2 (Figure 1F). This is likely due to the relocation of the dye from the bilayer surface (the location giving rise to the short component τ_1) to the tail region locations within the plasma membrane (characterised by the long component τ_2).

KNA exhibits a high triplet state yield (82% [65]) independent of viscosity [66], and the triplet state is able to react not only with oxygen [17, 18] with rate constant 2.3×10^9 M^{-1} s^{-1} [15], but also with amino acid residues of tryptophan and tyrosine with rate constants 2.5×10^9 M^{-1} s^{-1} and 0.8×10^9 M^{-1} s^{-1} [15, 67], respectively, leading to the formation of corresponding radicals [15, 67, 68]. Due to high concentrations of proteins in an eye lens (up to 400 mg/ml [69]) and lower concentration of oxygen, even under air-saturated conditions, we expect the main reactions of KNA triplet state to be with proteins and not with oxygen, (see Section S4 of SI for additional details). Thus, these reactions are expected to initiate Type I photodamage. The viscosity decrease detected upon 710 nm irradiation above is also in line with the data seen as a result of Type I photodamage in model DOPC-based GUVs, upon radical generation by a known mixed Type I/Type II sensitiser Methylene Blue [29].

To confirm that a decrease in τ_2 value is due to KNA-mediated radical reactions, we carried out two control measurements, Figure S9. In the first experiment (Figure S9 of SI, right) a KNA-incubated eye lens section was exposed to a dose of radiation at 930 nm, analogously to our experiments on Type II photodamage (Figure 1A). In the second experiment the eye lens slice stained

with **B6++,** without KNA, was irradiated at 710 nm (Figure S7 of SI, left). In both experiments we observed a significant increase of both the fluorescence intensity and the τ_2 values from membranes in the irradiated area, which closely matched the data for Type II photodamage (Figures 1A, S6, S9 of SI).

The first control experiment shows the prevalence of Type II photodamage with the excitation at 930 nm, which was expected as KNA does not absorb one or two photon light of this wavelength [65]. Additionally, this data confirms that KNA does not inhibit Type II damage generated by 930 nm irradiation. The second control experiment demonstrated that the Type II photodamage can be initiated at 710 nm, as well as at 930 nm, and the direction of viscosity change is the opposite to the one observed upon 710 nm excitation in the presence of KNA. This indicates that 710 nm irradiation initiates different photoreactions in the presence and the absence of KNA. It also seems likely that Type II reactions are still contributing to the observed viscosity change upon 710 nm irradiation in the presence of KNA. Thus, the reduction of viscosity in these experiments can be underestimated, as it may be partially masked by Type II-mediated increase that is occurring simultaneously, (see SI for a comment). It is interesting to note that such simultaneous activation of both types of damage appears to result in a narrowing of τ_2 distribution (red curve) as compared to the non-irradiated values (grey curve). This agrees with previous results on model membrane systems, where a narrow histogram of **B10** lifetime (τ_2) was obtained upon the photolysis of Methylene Blue in DOPC, which is expected to initiate both types of photodamage, Type I and Type II [29].

The long lifetime component (τ_2) exhibits monotonic changes with exposure dose in both cases of photodamage (Figure S10 of SI), reaching values of τ_2(Type I) = 4.14 ± 0.17 ns and τ_2(Type II) = 4.54 ± 0.22 ns. Though Type I photodamage leads to relatively small changes in the τ_2 value, a distinct difference between two types of damage could be clearly seen. Both Type I and II damages lead to visible increase of A_2 value (Figure 1) that could be interpreted as a relocation of **B6++** from the outer surface of membrane to the tail region of the lipid bilayer. This may originate from higher solubility of hydrophobic **B6++** within damaged membrane.

Radical reactions of KNA with amino acids and proteins were recently studied in detail, [16, 68, 70-72] however, there is no data regarding reactions of photoexcited KNA with lipids. It is important to note that the oxidation of $KNA^{\bullet-}$ by residual oxygen leads to the formation of superoxide anion $O_2^{\bullet-}$ [68, 71], which is typically considered as a precursor of other reactive oxygen species like hydrogen peroxide and hydroxyl radical [57]. The recombination reactions between tryptophanyl and tyrosyl radicals within protein globule result in the cross-linking of lens proteins [15,16]. It could be expected that under UV-A light KNA directly reacts with proteins from the intracellular space and, to a lesser extent, with membrane proteins. Subsequent radical reactions damage the most vulnerable cell constituents, including the unsaturated bonds of membrane lipids. The exact mechanisms of membrane damage in Type I reactions are not completely clear at present. It seems likely that radicals formed in the primary reactions of triplet state quenching by tryptophan and tyrosine residues of proteins are participating in a variety of reactions with surrounding proteins and unsaturated lipids from membranes. A formation of pores was previously reported [54, 73, 74] and we and others have previously reported an increase in membrane fluidity under Type I photodamage [29, 75]. It is likely that a cleavage of unsaturated bonds due to hydrogen abstraction increases the heterogeneity of membrane and lowers its viscosity. A cross-linking between lipids or between lipids and proteins may also contribute to the membrane heterogeneity, although we expect that the formation of cross-linked species should increase the viscosity [76].

Another interesting result is the change in the morphology of intracellular space upon Type I photodamage, namely the formation of granular inclusions stained with **B6++,** Figure 1C, 1D (for

high resolution intensity and FLIM images see Figures S6D1 and S6D2 of SI). The relocation of mainly hydrophobic **B6++** molecule from membranes to the intracellular space indicates a hydrophobic character of these structures. At the same time, the long lifetime of the rotor (that exceeds that expected from lipid membranes, Figures S6E-S6H of SI) indicates that it may be tightly bound. Our data cannot identify the content of these granules, but their location within intracellular milieu points out an inclusion of lens proteins. The proteins are known to lose water solubility upon aggregation and cross-linking [77-79], which is the major outcome of KNA-mediated damage to proteins via Type I radical reactions [15, 16]. Therefore, KNA induced Type I reactions may initiate the formation of these granules. Water insoluble protein aggregates likely contain hydrophobic domains, which could be suitable for binding of our rotor, which otherwise has a very poor solubility in an aqueous environment. If our assignment is correct, this is the first direct observation of protein aggregation within eye lens (*ex vivo*) under UV-A radiation.

The simulation of age-related photodamage to plasma membranes

In the living organism the eye lens is essentially an oxygen-free tissue [19] and it follows that any physiologically relevant studies of photodamage should be performed under anaerobic conditions and, ideally, in an intact lens. However, photolysis under aerobic conditions could provide additional mechanistic information about possible mechanisms for photoreactions taking place within tissue under UV-A irradiation and/or simulate the conditions of an eye trauma accompanied by an influx of oxygen.

We used the whole porcine eye lenses to study the effects of UV-A irradiation, simulating a natural light exposure-triggered ageing process. In these experiments a freshly harvested lens was placed in a quartz cuvette filled with the artificial aqueous humor (AAH), a liquid similar to that surrounding a lens in the living eye, and irradiated the sample by pulsed laser excitation at 355 nm under anaerobic or aerobic conditions (see Experimental section for details). In a control experiment another eye lens was kept at identical anaerobic conditions but without UV-A irradiation.

Characteristic FLIM images of thus treated and sliced tissues stained with **B6++** are shown in Figure 3. Identical biexponential decays of **B6++** within plasma membranes and a full coincidence of averaged histograms for control and untreated lenses (Figure 3G) indicates that the structure and properties of plasma membranes were unaffected by the prolonged stay of eye lens in AAH under anaerobic conditions.

UV-A irradiation leads to drastic changes in the fluorescence decays of **B6++** in eye lens tissue, Figure 3G. Analysis of the FLIM data shows that UV-A photolysis leads to minor variations in τ_1 values (Figure 3H) but significant lowering of the τ_2 values, indicative of lower viscosity (Figure 3I). Homogeneous distributions of τ_2 values over FLIM images (Figures 3D-3F) indicate no selectivity of photoinduced processes to different parts of cell membranes. The significant reduction in τ_2 values correlates well with changes seen in the case of Type I photodamage to eye lens membranes in this work and in model GUV membranes composed of DOPC [29].

Conversely, a slight increase of τ_2 values was seen under air-saturated conditions, Figure 3. This effect could be interpreted as a combined action of Type I and II photoreactions with a prevalence of Type II reactions in the total damage of plasma membrane. This indicates that at least a part of intrinsic eye lens chromophores form triplet states, which could be quenched by dissolved oxygen, leading to the formation of singlet oxygen. We note that these changes occurred in the absence of **B6++** and hence any damage was generated solely by the endogenous chromophores of the lens.

However, significant contribution of the Type I damage is seen even in the presence of oxygen. Under anaerobic conditions oxygen is not available and so the triplet states generated by 355 nm photolysis must react with surrounding tissue components initiating Type I damage to membranes *via* cascades of radical reactions. It should be noted that NAP(D)H is able to undergo two-photon ionization under UV-A light [80]. Though the probability of this process under natural conditions is very small, the photoionization leads to the formation of hydrated electron, a highly reactive species, which can oxidize surrounding molecules non-selectively.

Our results shed light on mechanisms of photoinduced processes in aerobic and anaerobic conditions within the eye lens and could be useful for the interpretation of age-related changes in the properties of plasma membranes of human eye lenses. However, it should be noted that the photoinduced changes observed in this work were recorded under conditions of an overloaded protection system. We used UV-A radiation intensities significantly higher than those expected to occur naturally and, thus, various processes, which normally should be supressed by main eye lens antioxidants present in the tissue (*e.g.* Asc and GSH) could not be effectively scavenged.

Other processes, such as slow thermal reactions initiated by photoinduced processes cannot be seen in our simple simulation experiment. For example, it was reported that UV-A photolysis of KN and lens proteins in the presence of Asc and subsequent incubation of irradiated samples under dark conditions during 3-7 days results in the formation of advanced glycation end products, which absorb UV-A light and contribute to the development of cataract [81]. However, these slow modification processes, that naturally take place on the timescales from several months to decades are difficult to simulate under laboratory conditions.

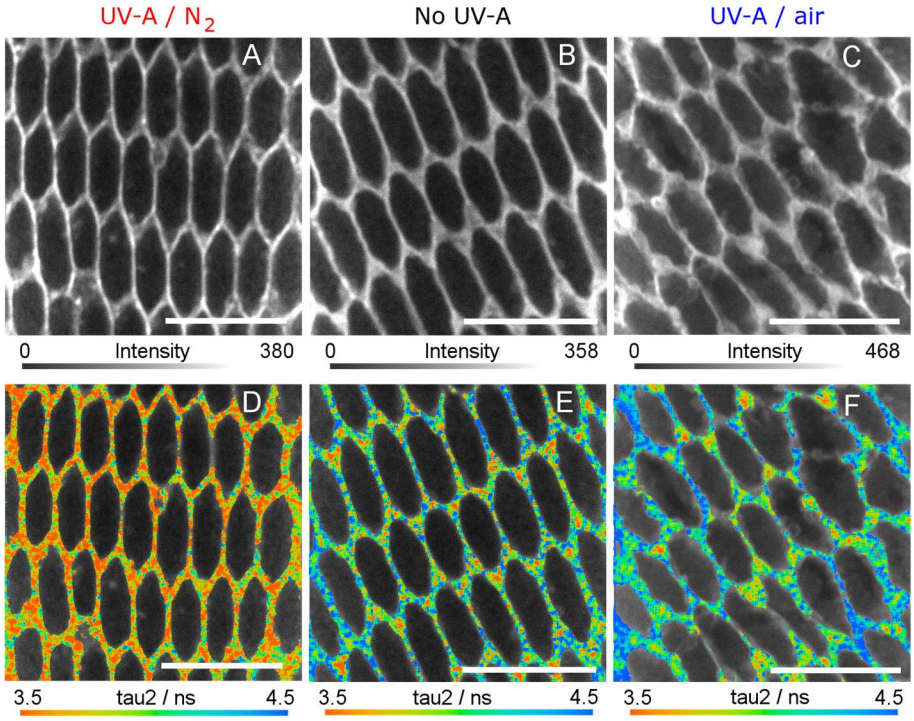

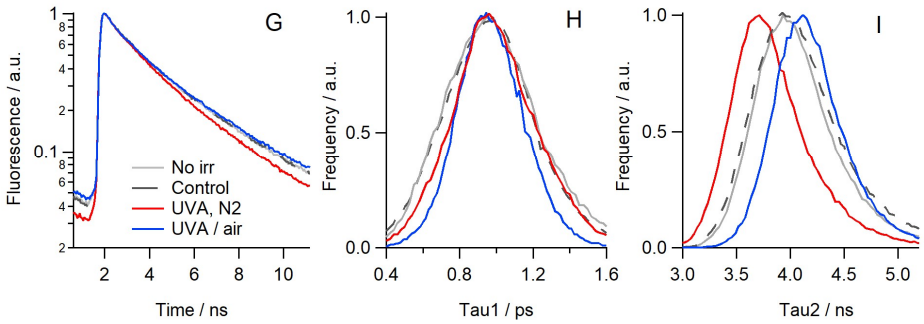

Figure 3. Fluorescence intensity (A-C) and FLIM (D-F) images of porcine eye lens stained with 10 μM **B6++**, following 355 nm irradiation of the whole lenses for 30 min (at 3 mJ/pulse, 10 Hz) under (A, D) anaerobic or (C, F) aerobic conditions; (B, E) control eye lens exposed to anaerobic conditions without UV-A light. Scale bars are 10 μm. (G-I) FLIM analysis of the data. (G) Averaged time-resolved decays recorded for **B6++** from randomly selected plasma membrane locations. Distributions of τ_1 (H) and τ_2 (I) from biexponential fits of FLIM data. No irradiation (grey dashed lines), control lens after staining under anaerobic conditions (light grey lines), 355 nm irradiation under anaerobic (red lines) and aerobic (blue lines) conditions. Independent biological experiments were performed in triplicate, four image frames were recorded per experiment.

Finally, we should mention that the lipid composition of plasma membranes of human eye lenses significantly differs from porcine samples, mainly by higher content of cholesterol and dihydro-sphingomyelins present in human lens membranes [25, 26, 32]. The composition of intracellular milieu is also somewhat different, for proteins [69] and metabolites [12, 46]. However, our results clearly show that changes in viscosity upon Type I and II damage to porcine eye lens membranes correlate well with changes observed within the model DOPC membranes [29], which are much less ordered and exhibit lower viscosity as compared to porcine lens membranes. Therefore, in the case of a human lens we could expect the same changes in viscosity in response to different photodamage types, although the extent of changes may vary from the values reported in this work.

Conclusions

In this work, we demonstrated that our approach, a combination of FLIM and molecular rotors, could be used to successfully quantify dynamic changes in viscosity within plasma membranes of eye lens under various types of photodamage. Type II photodamage results in significant increase of membrane viscosity that is expected to affect the transport of metabolites within this avascular tissue. Though intrinsic antioxidants Asc, GSH and α-tocopherol could prevent this photodamage to an extent, the maintenance of anaerobic conditions within the eye lens is critically important to avoid Type II reactions within the tissue.

In this work we studied the reactions initiated by multiphoton irradiation of KNA directly within the eye lens tissue, rather than in a diluted solution *in vitro,* for the first time. We demonstrated that irradiation of KNA within eye lens at 710 nm leads to Type I reactions, resulting in the damage to both intracellular proteins and lipid membranes. The evidence for the former was in the formation of hydrophobic substructures within intracellular milieu of eye lens cells; the latter was manifested by the lowering of the bilayer viscosity. For plasma membranes this outcome likely originates from radical induced cleavage of unsaturated bonds in lipids. Since KNA is known as a sensitizer of protein cross-linking, it seems reasonable to assume an additional contribution from cross-linking between lipids and proteins (trans-membrane and intracellular), however, more detailed studies at the molecular level are required to understand the nature of viscosity lowering in Type I photoreactions.

In our simulation of UV-A induced damage to the whole eye lens, we found that under anaerobic conditions the intrinsic eye lens constituents are able to generate damage to membranes with the lowering of membrane viscosity, which is characteristic of Type I photodamage. Due to a large variety of intrinsic chromophores susceptible to the UV-A light present within the eye lens, it is impossible to assign this effect to a particular chromophore or a reaction. Small increase of membrane viscosity during the photolysis under aerobic conditions was also seen, which probably could be attributed to a combined action of Type I and Type II reactions. Due to a very low oxygen pressure in an intact eye lens, Type II reactions are unlikely to prevail under normal conditions, apart from in an eye trauma.

It seems likely that Type I reactions are effectively inhibited in a healthy lens under natural conditions by intrinsic antioxidants. However, the impact of Type I reactions may be significantly increased with age and subsequent weakening of the protection system of an individual.

Acknowledgements

This work was supported by European Commission in the form of Individual Marie Sklodowska-Curie Fellowship to P.S.S. The initial stage of this work and the harvesting of animal eye lenses were supported by Russian Scientific Foundation (project #18-73-10014). M.K.K. is thankful to the EPSRC for a Career Acceleration Fellowship (EP/I003983/1). A.V. acknowledges travel grant from the Research Council of Lithuania (09.3.3.-LMT-K-712-07-0015).

Conflict of interest

There are no conflicts to declare.

References

1. Duane's Ophthalmology, 2007, Ed. W. Tasman, E.A. Jaeger, Ch.15, Williams & Wilkins, Philadelphia, USA.
2. N. Lynnerup, H. Kjeldsen, S. Heegaard, C. Jacobsen, J. Heinemeier, Radiocarbon dating of the human eye lens crystallins reveal proteins without carbon turnover throughout life, PLoSOne, 3 (2008) e1529. DOI: 10.1371/journal.pone.0001529.
3. J.R. Hughes, V.A. Levchenko. S.J. Blanksby, T.W. Mitchell, A. Willams, R.J.W. Truscott, No turnover in lens lipids for the entire human lifespan, eLife, 4 (2015) e06003. DOI: 10.7554/eLife.06003
4. M. H. J. Sweeney, R. J. W. Truscott, An impediment to glutathione diffusion in older normal human lenses: a possible precondition for nuclear cataract, Exp. Eye Res., 67 (1998) 587. DOI: 10.1006/exer.1998.0549.
5. B. A. Moffat, K. A. Landman, R. J. W. Truscott, M. H. J. Sweeney, J. M. Pope, Age-related changes in the kinetics of water transport in normal human lenses, Exp. Eye Res., 69 (1999) 663. DOI: 10.1006/exer.1999.0747
6. R. J. W. Truscott, Age-related nuclear cataract—oxidation is the key. Exp. Eye Res., 80 (2005) 709–725. DOI: 10.1016/j.exer.2004.12.007
7. J. M. Deeley, J. A. Hankin, M. G. Friedrich, R. C. Murphy, R. J. W. Truscott, T. W. Mitchell, S. J. Blanksby, Sphingolipid distribution changes with age in the human lens, J. Lipid Res., 51 (2010) 2753–2760. DOI: 10.1194/jlr.M007716
8. J. R. Hughes, J. M. Deeley, S. J. Blanksby, F. Leisch, Sh. R. Ellis, R. J. W. Truscott, T. W. Mitchell, Instability of the cellular lipidome with age, Age, 34 (2012) 935–947. DOI: 10.1007/s11357-011-9293-6

9. G. T. Wondrak, M. K. Jacobson, E. L. Jacobson, Endogenous UVA-photosensitizers: mediators of skin photodamage and novel targets for skin photoprotection, Photochem. Photobiol. Sci., 5 (2006) 215-237. DOI: 10.1039/B504573H.
10. F. J. Giblin, V. R. Leverenz, V. A. Padgaonkar, N. J. Unakar, L. Dang, L. R. Lin, M. F. Lou, V. N. Reddy, D. Borchman, J.P. Dillon, UVA light *in vivo* reaches the nucleus of the guinea pig lens and produces deleterious, oxidative effects, Exp. Eye Res., 75 (2002) 445–458. DOI: 10.1006/exer.2002.2039
11. L. M. Bova, M. H. Sweeney, J. F. Jamie, R. J. W. Truscott, Major changes in human ocular UV protection with age, Invest. Ophthalmol. Vis. Sci., 42 (2001) 200-205. PubMed ID:11133868.
12. Yu. P. Tsentalovich, T. D. Verkhovod, V. V. Yanshole, A. S. Kiryutin, L. V. Yanshole, A. Z. Fursova, D. A. Stepakov, V. P. Novoselov, R. Z. Sagdeev, Metabolomic composition of normal aged and cataractous human lenses, Exp. Eye Res., 134 (2015) 15–23. DOI: 10.1016/j.exer.2015.03.008.
13. P.S. Sherin, Yu.P. Tsentalovich, O.A. Snytnikova, R.Z. Sagdeev, Photoactivity of kynurenine-derived UV filters, J. Photochem. Photobiol. B: Biol., 93 (2008) 127-132. DOI: 10.1016/j.jphotobiol.2008.07.006.
14. Yu. P. Tsentalovich, P. S. Sherin, L. V. Kopylova, I. V. Cherepanov, J. Grilj, E. Vauthey, Photochemical properties of UV filter molecules of the human eye, Invest. Ophthalmol. Vis. Sci., 52 (2011) 7687-7696. DOI: 10.1167/iovs.11-8120.
15. P. S. Sherin, E. A. Zelentsova, E. D. Sormacheva, V. V. Yanshole, T. G. Duzhak, Yu. P. Tsentalovich, Aggregation of α-crystallins in kynurenic acid-sensitized UVA photolysis under anaerobic conditions, Phys. Chem. Chem. Phys., 18 (2016) 8827-8839. DOI: 10.1039/C5CP06693J.
16. E. D. Savina, Yu. P. Tsentalovich, P. S. Sherin, UV-A induced damage to lysozyme via Type I photochemical reactions sensitized by kynurenic acid, Free Rad. Biol. Med., 152 (2020) 482-493. DOI: 10.1016/j.freeradbiomed.2019.11.017
17. S. I. Egorov, M. A. Babizhaev, A. A. Krasnovskii Jr., A. A. Shvedova, Photosensitized generation of singlet molecular oxygen by endogenous substances of the eye lens, Biofizika. 32 (1987) 169–171. PubMedID: 3814638
18. C. M. Krishna, S. Uppuluri, P. Riesz, J. S. Zigler Jr., D. Balasubramanian, A study of the photodynamic efficiencies of some eye lens constituents, Photochem. Photobiol., 54 (1991) 51–58. DOI: 10.1111/j.1751-1097.1991.tb01984.x
19. R. McNulty, H. Wang, R. T. Mathias, B. J. Ortwerth, R. J. W. Truscott, S. Bassnett, Regulation of tissue oxygen levels in the mammalian lens, J Physiol., 559 (2004) 883-898. DOI: 10.1113/jphysiol.2004.068619.
20. P. S. Sherin, I. Lopez-Duarte, M. R. Dent, M. Kubankova, A. Vyšniauskas, J. A. Bull, E. S. Reshetnikova, A. S. Klymchenko, Yu. P. Tsentalovich, M. K. Kuimova, Visualising the membrane viscosity of porcine eye lens cells using molecular rotors, Chem. Sci. 8 (2017) 3523-3528. DOI: 10.1039/c6sc05369f
21. M. K. Kuimova, G. Yahioglu, J. A. Levitt, K. Suhling, Molecular rotor measures viscosity of live cells via fluorescence lifetime imaging, J. Am. Chem. Soc. 130 (2008) 6672. DOI: 10.1021/ja800570d
22. M. R. Dent, I. López-Duarte, C. J. Dickson, P. Chairatana, H. L. Anderson, I. R. Gould, D. Wylie, A. Vyšniauskas, N. J. Brooks, M. K. Kuimova, Imaging plasma membrane phase behaviour in live cells using a thiophene-based molecular rotor, Chem. Comm. 52 (2016) 13269. DOI: 10.1039/C6CC05954F

23. M. Kubánková, P.A. Summers, I. López-Duarte, D. Kiryushko, M.K. Kuimova, Microscopic viscosity of neuronal plasma membranes measured using fluorescent molecular rotors: effects of oxidative stress and neuroprotection, ACS Appl. Mater. Interfaces 11 (2019) 36307–36315. DOI: 10.1021/acsami.9b10426
24. A. S. Kashirina, I. López-Duarte, M. Kubánková, A. A. Gulin, V. V. Dudenkova, S. A. Rodimova, H. G. Torgomyan, E. V. Zagaynova, A. V. Meleshina, M. K. Kuimova, Monitoring membrane viscosity in differentiating stem cells using BODIPY-based molecular rotors and FLIM, Sci. Rep., 10 (2020) 14063. DOI: 10.1038/s41598-020-70972-5
25. J. M. Deeley, T. W. Mitchell, X. Wei, J. Korth, J. R. Nealon, S. J. Blanksby, R. J. W. Truscott, Human lens lipids differ markedly from those of commonly used experimental animals, Biochim. Biophys. Acta, 1781 (2008) 288. DOI: 10.1016/j.bbalip.2008.04.002
26. D. Borchman, Lipid conformational order and the etiology of cataract and dry eye, J. Lipid. Res. 61 (2021) 100039. DOI: 10.1194/jlr.TR120000874
27. M. K. Kuimova, S. W. Botchway, A. W. Parker, M. Balaz, H. A. Collins, H. L. Anderson, K. Suhling and P. R. Ogilby, Imaging intracellular viscosity of a single cell during photoinduced cell death, Nat. Chem., 1 (2009) 69–73. DOI: 10.1038/nchem.120
28. M. A. Izquierdo, A. Vyšniauskas, S. A. Lermontova, I. S. Grigoryev, N. Y. Shilyagina, I. V. Balalaeva, L. G. Klapshina M. K. Kuimova, Dual use of porphyrazines as sensitizers and viscosity markers in photodynamic therapy, J. Mat. Chem. B, 3 (2015) 1089-1096. DOI: 10.1039/c4tb01678e
29. A. Vyšniauskas, M. Qurashi, M. K. Kuimova, A molecular rotor that measures dynamic changes of lipid bilayer viscosity caused by oxidative stress, Chem. Eur. J., 22 (2016) 13210 – 13217. DOI: 10.1002/chem.201601925
30. I. López-Duarte, T. T. Vu, M. A. Izquierdo, J. A. Bull, M. K. Kuimova, A molecular rotor for measuring viscosity in plasma membranes of live cells, Chem. Comm., 50 (2014) 5282. DOI: 10.1039/c3cc47530a
31. E. M. Woodcock, P. Girvan, J. Eckert, I. Lopez-Duarte, M. Kubankova, J. J. W. A. van Loon, N. J. Brooks, M. K. Kuimova, Measuring intracellular viscosity in conditions of hypergravity, Biophys. J., 116 (2019) 1984-1993. DOI: 10.1016/j.bpj.2019.03.038
32. M. C. Yappert, M. Rujoi, D. Borchman, I. Vorobyov, R. Estrada, Glycero- versus sphingo-phospholipids: correlations with human and non-human mammalian lens growth, Exp. Eye Res., 76 (2003) 725. DOI: 10.1016/S0014-4835(03)00051-4
33. C. Marti, O. Jürgens, O. Cuenca, M. Casals, S. Nonell, Aromatic ketones as standards for singlet molecular oxygen photosensitization. Time-resolved photoacoustic and near-IR emission studies, J. Photochem. Photobiol., A: Chem., 97 (1996) 11-18. DOI: 10.1016/1010-6030(96)04321-3
34. R. D. Scurlock, D. O. Martire, P. R. Ogilby, V. L. Taylor, R. L. Clough, Quantum yield of photosensitized singlet oxygen production in solid polystyrene, Macromolecules, 27 (1994) 4787-4794. DOI: 10.1021/ma00095a020
35. P. Salice, J. Arnbjerg, B. W. Pedersen, R. Toftegaard, L. Beverina, G. A. Pagani, P. R. Ogilby Photophysics of squaraine dyes: role of charge-transfer in singlet oxygen production and removal, J. Phys. Chem. A, 114 (2010), 2518–2525. DOI: 10.1021/jp911180n.
36. W. Becker, The BH TCSPC Handbook, 8th Edition, September 2019, p. 783. https://www.becker-hickl.com/literature/documents/flim/the-bh-tcspc-handbook/
37. M. K. Kuimova, Mapping viscosity in cells using molecular rotors, Phys. Chem. Chem. Phys., 14 (2012) 12671-12686. DOI: 10.1039/c2cp41674c

38. L. E. Shimolina, M. A. Izquierdo, I. López-Duarte, J. A. Bull, M. V. Shirmanova, L. G. Klapshina, E. V. Zagaynova, M. K. Kuimova, Imaging tumor microscopic viscosity in vivo using molecular rotors, Sci. Rep. 7 (2017) 41097. DOI: 10.1038/srep41097
39. M. V. Shirmanova, L. E. Shimolina, M. M. Lukina, E. V. Zagaynova, M. K. Kuimova, Live cell imaging of viscosity in 3D tumour cell models, In: Dmitriev R. (eds) Multi-Parametric Live Cell Microscopy of 3D Tissue Models. Advances in Experimental Medicine and Biology, vol 1035. Springer, Cham. DOI: 10.1007/978-3-319-67358-5_10
40. M. R. Dent, I. López-Duarte, C. J. Dickson, N. D. Geoghegan, J. M. Cooper, I. R. Gould, R. Krams, J. A. Bull, N. J. Brooks, M. K. Kuimova, Imaging phase separation in model lipid membranes through the use of BODIPY based molecular rotors, Phys. Chem. Chem. Phys., 17 (2015) 18393. DOI: 10.1039/C5CP01937K
41. F. Wilkinson, W. P. Helman, A. B. Ross, Rate constants for the decay and reactions of the lowest electronically excited singlet state of molecular oxygen in solution. An expanded and revised compilation, J. Phys. Chem. Ref. Data, 24 (1995) 663–1021. DOI: 10.1063/1.555965.
42. M. Bregnhøj, M. Westberg, B. F. Minaev, P. R. Ogilby, Singlet Oxygen Photophysics in Liquid Solvents: Converging on a Unified Picture. Acc. Chem. Rev., 50 (2017) 1920-1927. DOI: 10.1021/acs.accounts.7b00169
43. P. Dongare, S. Maji, L. Hammarström, Direct evidence of a tryptophan analogue radical formed in a concerted electron−proton transfer reaction in water, J. Am. Chem. Soc., 138 (2016) 2194-2199. DOI: 10.1021/jacs.5b08294
44. A. Baj, J. Cedrowski, E. Olchowik-Grabarek, A. Ratkiewicz, S. Witkowski, Synthesis, DFT calculations, and in vitro antioxidant study on novel carba-analogs of vitamin E, Antioxidants, 8 (2019) 589. DOI: 10.3390/antiox8120589
45. R. J. W. Truscott, Human age-related cataract: a condition with no appropriate animal model, J. Clinic. Experiment. Ophthalmol., 2 (2011) 8. DOI: 10.4172/2155-9570.1000178
46. V. V. Yanshole, O. A. Snytnikova, A. S. Kiryutin, L. V. Yanshole, R. Z. Sagdeev, Yu. P. Tsentalovich, Metabolomics of the rat lens: A combined LC-MS and NMR study, Exp. Eye Res., 125 (2014) 71-78. DOI: 10.1016/j.exer.2014.05.016.
47. J. Tornmalm, E. Sandberg, M. Rabasovic, J. Widengren, Local redox conditions in cells imaged via non-fluorescent transient states of NAD(P)H, Sci. Rep., 9 (2019) 15070. DOI: 10.1038/s41598-019-51526-w
48. E. A. Zelentsova, L. V. Yanshole, A. Z. Fursova, Yu. P. Tsentalovich, Optical properties of the human lens constituents, J. Photochem. Photobiol. B Biol., 173 (2017) 318−324. DOI: 10.1016/j.jphotobiol.2017.06.005
49. A. Kamkaew, S. H. Lim, H. B. Lee, L. V. Kiew, L. Y. Chung, K. Burgess, BODIPY dyes in photodynamic therapy, Chem. Soc. Rev., 42 (2013) 77-88. DOI: 10.1039/C2CS35216H
50. J. Zhao, K. Xu, W. Yang, Z. Wang, F. Zhong, The triplet excited state of Bodipy: formation, modulation and application, Chem. Soc. Rev., 44 (2013) 8904-8939. DOI: 10.1039/C5CS00364D
51. R. Galli, O. Uckermann, E. F. Andresen, K. D. Geiger, E. Koch, G. Schackert, G. Steiner, M. Kirsch, Intrinsic indicator of photodamage during label-free multiphoton microscopy of cells and tissues, PLOS One, 9 (2014) e110295. DOI: 10.1371/journal.pone.0110295
52. S. N. Arkhipov, I. Saytashev, M. Dantus, Intravital imaging study on photodamage produced by femtosecond near-infrared laser pulses in vivo, Photochem. Photobiol., 92 (2016) 308-313. DOI: 10.1111/php.12572

53. K. A. Riske, T. P. Sudbrack, N. L. Archilha, A. F. Uchoa, A. P. Schroder, C. M. Marques, M. S. Baptista, R. Itri, Giant vesicles under oxidative stress induced by a membrane-anchored photosensitizer, Biophys. J. 97 (2009) 1362–1370. DOI: 10.1016/j.bpj.2009.06.023
54. R. Itri, H. C. Junqueira, O. Mertins, M. S. Baptista, Membrane changes under oxidative stress: the impact of oxidized lipids, Biophys. Rev., 6 (2014) 47–61. DOI: 10.1007/s12551-013-0128-9
55. C. Banerjee, T. Breitenbach, P. R. Ogilby, Spatially resolved experiments to monitor the singlet oxygen initiated oxidation of lipid droplets in emulsions. Chem. Photo. Chem., 2 (2018) 586-595. DOI: 10.1002/cptc.201800005
56. H. Heath, The distribution and possible functions of ascorbic acid in the eye., Exp. Eye Res., 1 (1962) 362–367. DOI: 10.1016/S0014-4835(62)80025-6
57. A. Blázquez-Castro, M. Westberg, M. Bregnhøj, T. Breitenbach, D. J. Mogensen, M. Etzerodt, P. R. Ogilby, Chapter 19. Light-initiated oxidative stress, Oxidative Stress. Eustress and distress, (2020) 363-388. DOI: 10.1016/B978-0-12-818606-0.00019-5
58. O. A. Snytnikova, P. S. Sherin, L. V. Kopylova, Yu. P. Tsentalovich, Kinetics and mechanism of reactions of photoexcited kynurenine with molecules of some natural compounds, Russ. Chem. Bull. (Int. Ed.), 56 (2007) 732. DOI: 10.1007/s11172-007-0109-x.
59. P. S. Sherin, N. P. Gritsan, Yu. P. Tsentalovich, Experimental and quantum chemical study of photochemical propertiesof 4-hydroxyquinoline, Photochem. Photobiol. Sci., 8 (2009) 1550-1557. DOI: 10.1039/B9PP00017H.
60. F. J. Giblin, Glutathione: a vital lens antioxidant J. Ocul. Pharmacol. Ther., 2000 (16) 121. DOI: 10.1089/jop.2000.16.121
61. D. L. Williams, Oxidation, antioxidants and cataract formation: a literature review, Vet. Ophthalmol., 9 (2006) 292. DOI: 10.1111/j.1463-5224.2006.00498.x
62. W. Pendergrass, P. Penn, D. Possin, N. Wolf, Accumulation of DNA, nuclear and mitochondrial debris, and ROS at sites of age-related cortical cataract in mice, Invest. Ophthal. Vis. Sci., 46 (2005) 4661-4670. DOI:10.1167/iovs.05-0808
63. W.R. Pendergrass, P.E. Penn, D. E. Possin, N.S. Wolf, Cellular debris and ROS in age-related cortical cataract are caused by inappropriate involution of the surface epithelial cells into the lens cortex, Mol. Vis., 12 (2006) 712-724. http://www.molvis.org/molvis/v12/a80/
64. T. Zarnowski, R. Rejdak, Z. Zagorski, A. G. M. Juenemann, E. Zrenner, T. Kocki, E. M. Urbanska, W. A. Turski, Content of kynurenic acid and activity of kynurenine aminotransferases in mammalian eyes. Ophthalm. Res. 36 (2004) 124–128. DOI: 10.1159/000076893
65. E. A. Zelentsova, P. S. Sherin, O. A. Snytnikova, R. Kaptein, E. Vauthey, Yu. P. Tsentalovich, Photochemistry of aqueous solution of kynurenic acid and kynurenine yellow, Photochem. Photobiol. Sci., 12 (2013) 546-558. DOI: 10.1039/C2PP25357G.
66. E. A. Zelentsova, P. S. Sherin, Yu. P. Tsentalovich, R. Z. Sagdeev, Influence of medium viscosity on photophysical properties of kynurenic acid and kynurenine yellow, Russ. Chem. Bull., 66 (2017) 267-272. DOI: 10.1007/s11172-017-1727-6.
67. Yu. S. Zhuravleva, Yu. P. Tsentalovich, Acid-alkaline properties of triplet state and radical of kynurenic acid, J. Photochem. Photobiol. A: Chem. 365 (2018) 7-12. DOI: 10.1016/j.jphotochem.2018.07.029.
68. E. D. Sormacheva, P. S. Sherin, Yu. P. Tsentalovich, Dimerization and oxidation of tryptophan in UV-A photolysis sensitized by kynurenic acid, Free Rad. Biol. Med., 113 (2017) 372-384. DOI: 10.1016/j.freeradbiomed.2017.10.007.

69. H. Bloemendal, W. De Jong, R. Jaenicke, N. H. Lubsen, C. Slingsby, A. Tardieu, Ageing and vision: structure, stability and function of lens crystallins, Progr. Biophys. Mol. Biol., 86 (2004) 407-485. DOI: 10.1016/j.pbiomolbio.2003.11.012.
70. Yu. S. Zhuravleva, O. B. Morozova, Yu. P. Tsentalovich, P. S. Sherin, Proton-coupled electron transfer as the mechanism of reaction between triplet state of kynurenic acid and tryptophan, J. Photochem. Photobiol. A.: Chem., 396 (2020) 112522. DOI: 10.1016/j.jphotochem.2020.112522.
71. Yu. S. Zhuravleva, P. S. Sherin, Influence of pH on radical reactions between kynurenic acid and amino acids tryptophan and tyrosine. Part I. Amino acids in free state, Free Rad. Biol. Med., 172 (2021) 331-339, DOI: 10.1016/j.freeradbiomed.2021.06.015
72. Yu. S. Zhuravleva, P. S. Sherin, Influence of pH on radical reactions between kynurenic acid and amino acids tryptophan and tyrosine. Part II. Amino acids within the protein globule of lysozyme, Free Rad. Biol. Med., 174 (2021) 211-224, DOI: 10.1016/j.freeradbiomed.2021.08.001
73. S. Sankhagowit, S. H. Wu, R. Biswas, C. T. Riche, M. L. Povinelli, N. Malmstadt, The dynamics of giant unilamellar vesicle oxidation probed by morphological transitions, Biochim. Biophys. Acta Biomembr., 1838 (2014) 2615–2624. DOI: 10.1016/j.bbamem.2014.06.020
74. O. Mertins, I. O. L. Bacellar, F. Thalmann, C. M. Marques, M. S. Baptista, R. Itri, Physical damage on giant vesicles membrane as a result of methylene blue photoirradiation, Biophys. J. 106 (2014) 162–171. DOI: 10.1016/j.bpj.2013.11.4457
75. W. Y. Tai, Y. C. Yang, H. J. Lin, C. P. Huang, Y. L. Cheng, M. F. Chen, H. L. Yen, I. Liau, Interplay between structure and fluidity of model lipid membranes under oxidative attack, J. Phys. Chem. B, 114 (2010) 15642–15649. DOI: 10.1021/jp1014719
76. N. A. Hosny, C. Fitzgerald, A. Vyšniauskas, A. Athanasiadis, T. Berkemeier, N. Uygur, U. Pöschl, M. Shiraiwa, M. Kalberer, F. D. Pope, M. K. Kuimova, Direct imaging of changes in aerosol particle viscosity upon hydration and chemical aging, Chem. Sci., 7 (2016) 1357-1367. DOI: 10.1039/C5SC02959G
77. V. Harrington, S. McCall, S. Huynh, K. Srivastava, O.P. Srivastava, Crystallins in water soluble-high molecular weight protein fractions and water insoluble protein fractions in aging and cataractous human lenses, Mol. Vis. 10 (2004) 476–489. PMID: 15303090
78. K. L. Schey, Z. Wang, M. G. Friedrich, D. L. Garland, R. J. W. Truscott, Spatiotemporal changes in the human lens proteome: Critical insights into long-lived proteins, Progr. Ret. Eye Res., 76 (2020) 100802. DOI: 10.1016/j.preteyeres.2019.100802
79. T. Grune, Oxidized protein aggregates: Formation and biological effects, Free Rad. Biol. Med. 150 (2020) 120-124. DOI: 10.1016/j.freeradbiomed.2020.02.014
80. L. Lindqvist, B. Czochralska, I. Grigorov, Determination of the mechanism of photoionization of NADH in aqueous-solution on laser excitation at 355 nm. Chem. Phys. Lett., 119 (1985) 494–498. DOI: 10.1016/0009-2614(85)85375-6
81. M. Linetsky, C.T. Raghavan, K. Johar, X. Fan, V.M. Monnier, A.R. Vasavada, R.H. Nagaraj, UVA light-excited kynurenines oxidize ascorbate and modify lens proteins through the formation of advanced glycation end products: implications for human lens aging and cataract formation, J. Biol. Chem., 289 (2014) 17111-17123. DOI: 10.1074/jbc.M114.554410.

Figure captions

Figure 1. (A, C) Intensity and (B, D) FLIM images of porcine eye lens stained with 10 μM **B6++** following (A, B) 930 nm irradiation or (C, D) in the presence of 3 mM KNA following 710 nm irradiation. The central frame was irradiated for 1400 sec at 2.0 mW power at the wavelength indicated, the whole image acquisition time was 300 sec at 0.45 mW. Scale bars are 10 μm. (E-H) FLIM analysis of the data. (E) Averaged time-resolved decays recorded for **B6++** from randomly selected plasma membrane locations (see Section S1 of SI for additional details). Distributions of τ_1 (F), τ_2 (G) and A_2 (H) obtained from biexponential fits of FLIM data. No irradiation (grey lines), 930 nm irradiation (red lines) and 710 nm irradiation in the presence of KNA (blue lines). Independent biological experiments were performed in triplicate, two image frames were analysed per experiment. Full size images are presented in Figure S6 of SI.

Figure 2. Intensity (A) and FLIM (B) images of porcine eye lens stained with 10 μM **B6++** and 3 mM Asc following 930 nm irradiation. The central frame was irradiated for 1400 sec (at 2.0 mW power), the whole image acquisition time was 300 sec (at 0.45 mW). Scale bars are 10 μm. (C-F) Distributions of τ_2 obtained from biexponential fits of FLIM data. Before (solid grey) and after (dashed grey lines) photolysis at 930 nm in the absence and presence of (C) D_2O (red lines), (D) 10 μM of α-tocopherol (blue lines), (E) 10 mM (green lines) and 40 mM (olive lines) NaN_3, (F) 3 mM Asc (orange) and 3 mM GSH (violet). Independent biological experiments were performed in duplicate, two image frames were analysed per experiment.

Figure 3. Fluorescence intensity (A-C) and FLIM (D-F) images of porcine eye lens stained with 10 μM **B6++**, following 355 nm irradiation of the whole lenses for 30 min (at 3 mJ/pulse, 10 Hz) under (A, D) anaerobic or (C, F) aerobic conditions; (B, E) control eye lens exposed to anaerobic conditions without UV-A light. Scale bars are 10 μm. (G-I) FLIM analysis of the data. (G) Averaged time-resolved decays recorded for **B6++** from randomly selected plasma membrane locations. Distributions of τ_1 (H) and τ_2 (I) from biexponential fits of FLIM data. No irradiation (grey dashed lines), control lens after staining under anaerobic conditions (light grey lines), 355 nm irradiation under anaerobic (red lines) and aerobic (blue lines) conditions. Independent biological experiments were performed in triplicate, four image frames were recorded per experiment.